Journal of Visualization, Vol. 8, No. 2 (2005)99-108

Vortex Shedding Process Investigation Downstream a Surface-Mounted Block

Calluaud, D. *, David, L.* and Texier, A.*

* Laboratoire d'Etudes Aérodynamiques (UMR 6609-CNRS) Boulevard Pierre et Marie Curie Téléport 2, B.P. 30179 86960 FUTUROSCOPE POITIERS Cedex, France.

Received 1 September 2004
Revised 8 November 2004

Abstract: The laminar flow around a surface-mounted block is investigated by visualizations and PIV measurements. Flow topology and, especially, the vortex shedding dynamics are emphasized. The existence of two vortex shedding processes is highlighted by particles visualizations and instantaneous velocity fields analyses. On one hand, a dominant swirling mechanism with vortex matching process and a symmetrical topology sets up and, on the other hand, a non periodical evolution with a dissymmetric topology exist. In order to inquire about those processes, double velocity correlation functions are calculated and from those new data the space and time evolutions of the vortices are detailed.

Keywords: Wake, Vortex dynamic, Velocimetry, Correlation, Visualization.

1. Introduction

Flows around surface-mounted three-dimensional bluff-bodies are characterized by a complex and three-dimensional topology: unsteady vortex structures, separation and reattachment regions. However full knowledge of these flow characteristics will be useful in a large variety of technological and useful applications such as the heat transfer phenomena around electronic components, wind loads on structures and building, dispersion of pollutants, etc.

Yet, the flow around surface-mounted obstacles was already experimentally and numerically investigated by different authors - Hunt et al. (1978), Castro and Robins (1977), Schofield and Logan (1990), Larousse et al. (1991), Martinuzzi and Tropea (1993), Rodi et al. (1997). Those studies have plainly shown the complexity of the flow around and more extensively behind a surface-mounted cube. According to this scientific literature, the flow field around a three-dimensional obstacle is characterized by different flow features. Upstream the model, a typical horseshoe vortex system caused by the adverse pressure gradient of the stagnating flow is observed. On the sides and the top of the box, typical recirculation regions and flow model face reattachments can be observed. Downstream the obstacle, a recirculation region evolves before merging in the wake. As part of this topic, Hunt et al. (1978), Castro and Robins (1977) and Castro and Diana (1983) highlight that the unsteady of the upstream horseshoe vortex, the reattachment of the separation region on the upper cube face, and the downstream recirculation region are dependent on the upstream turbulence intensity level and the model dimensions. However, most of those works have particularly described the mean surface mounted block flow topology, in other words a global feature of this flow. Even if time-averaged and mean flow properties provide sufficient information for a part of engineering applications, those approaches could not plainly explain the dynamic of this typical flow and

associated vortex formations evolutions and fluctuations.

The dynamic flow evolution, especially the vortex shedding process behind the obstacle is briefly explained by Martinuzzi et al. (1992) with help of Laser Doppler Velocimetry (LDV) measurements and bi-modal distribution of the velocity. Recently, Becker et al. (2002), Sousa (2002) and Calluaud and David (2004) have underlined the close connection that exists between the vortex shedding dynamic downstream the block and the distribution of the turbulence intensity. Moreover, Vlachos and Hajj (2002) with use of Particle Image Velocimetry (PIV) technique and instantaneous vorticity distributions emphasize the flow dynamic in the separation region and some associated instantaneous parameters.

In this work, the three-dimensional laminar flow over a surface-mounted block with a small aspect ratio is investigated. The entire physical principles and the time and space evolutions of the vortex shedding mechanism downstream the obstacle are revealed by analysis of flow visualizations, instantaneous 2C and 3C measurements and velocity fluctuation correlation calculations.

2. Experimental Setup

2.1 The Experimental Arrangement

The experiments were carried out in a hydrodynamic channel facility.

The channel operates in a closed loop with up to 1.5 m^3 of water. Ahead a settling chamber, a convergence leads to the 0.16 m × 0.16 m × 0.8m test section made of a clear, acrylic Altuglas. Three axial pumps drive the flow at a speed close to 0.1 $m.s^{-1}$. The block is 60 mm in diameter D and 18 mm in height H. It sets at X_0=40 mm of a flat plate leading edge which covers the whole width of the test section (Fig. 1) and extends to 4 diameters downstream the model. The Reynolds number bases on the D diameter and the U_0 uniform flow velocity is 1,000. The boundary layer thickness value at the block trailing edge is 0.43.H.

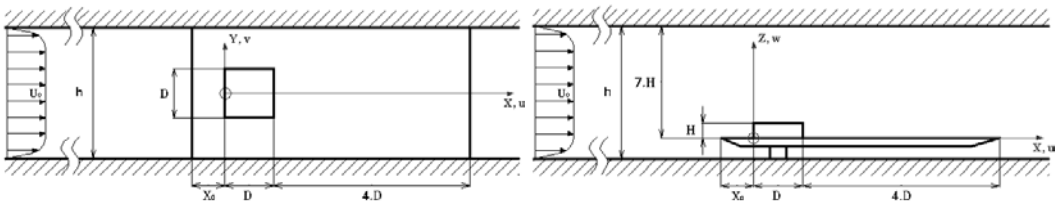

Fig. 1. Top (a) and side (b) views of the arrangement.

2.2 Measurement and Visualisation Techniques

Flow visualizations and three velocity component measurements by stereoscopic particle image velocimetry (SPIV) are performed to obtain the flow topology and to measure the complex and three dimensional movements of the full visualized flow field seeding with tiny hollow glass particles 15µm in diameter. The experiments were carried out for different sections of the flow domain: in span-planes (O/XZ) with Y/D=0, 1/2, 1/3, 1/6 and transverse planes (O/XY) with Z/D=0, 0.15, 0.3.

Particle streak flow field visualizations are done in different sections of the flow illuminated by means of a continuous laser (12 Watts Spectra Physics argon laser) sheet of 1 mm in thickness. A Nikon F4S camera with different lenses is used. During a short time exposure, some particle paths can give access to instantaneous streak fields which provide information on both flow topology and kinematics.

In order to appreciate the 3-D flow structure, a complementary visualization technique is used: the continuous dye-emission, based on a continuous electrolytic process of tin-ribbon.

2.3 Particle Image Velocimetry

The three components PIV setup consists of two Dantec 80C42 DoubleImage 700 cameras that give the stereo view of the seeding flow. The CCD cameras are 768 × 484 $pixels^2$ in resolution with an 8 bit dynamic range and a 30 Hz maximum frame rate. Both cameras hold lens of 105 mm fixed focal and

Scheimpflug table arrangement. In order to reduce the optical aberrations due to the passage through the air-altuglass-water dioptre, prisms filled with water are laid out against the faces of the hydrodynamics channel, as in Prasad and Jensen (1995).

In a typical angular measurement configuration the viewing angles of cameras 1 and 2 are fixed respectively at 45° and -45° relatively to the X axis. A doubled Nd-Yag laser (Quantel Mini-Yag Twin Ultra Blue Sky laser with 30 mJ/pulse) illuminates the flow field with a time period Δt about 40.0-50.0 ms between two pulses. The laser sheet thickness is about 3.5 mm to generate an equal spatial resolution in the three flow directions - Scarano (2003) -. The FlowMap 3.61 Dantec software synchronizes the double frame cameras and the laser pulses at 15 Hz. It allows to acquire up to 200 image pairs per camera. The two-dimensional velocity fields are computed with FlowMap software, by double frame image processing by an adaptive cross-correlation PIV analysis using FFT on final size 32×32 pixels^2 of windows with a 50 % overlap. In the last step of this iterative PIV analysis, two runs are performed to acquire a best sub-pixel approximation. The three components velocity fields result from a reconstruction algorithm based on 3D calibration - Prasad (2000) - according to a reference pinhole camera model method associates to an algorithm developed by Calluaud and David (2004). For this 2D-3C PIV configuration, with a resolution of 115µm/pixels, the authors have shown that the three dimensional displacement accuracy is about 6 µm according to each direction.

In order to lead to quantitative information on the evolution of the flow structures, three double velocity fluctuation correlation coefficients (time, space and spatio-temporal correlation coefficients) are calculated. For the two terms f and g in equation 1, the correlation coefficient R_{fg} is a number between -1 and 1 which displays the relationship level between f and g. A perfect linear relationship leads to a correlation coefficient equal to 1 or –1. Inversely a correlation coefficient of 0 means that there is no linear relationship between f and g.

$$R_{fg} = \left[\int_{-\infty}^{+\infty} \int f\, g\, P(f,g)\quad df\ dg \right] \Big/ \left[\sqrt{\overline{f^2}}\sqrt{\overline{g^2}} \right] \text{, with P (f, g) the function probability of f and g.} \qquad (1)$$

The temporal and spatial correlations is obtained using PIV measurements technique with 25 Hz acquisition rate. According to the flow dynamic and, more particularly, to the slow velocity convection of the vortices, the data resulting from those PIV measurements allows to obtain a sufficient time resolution which makes it possible to describe the phenomena generated in the obstacle wake.

3. Flow Topology and Dynamics

As a general rule, the main features of the mean flow structure around the investigated block obstacle are topologically similar to those around other cubic bluff-bodies for greater Reynolds numbers - Martinuzzi and Tropea (1993).

Upstream the block, a junction flow is established. A typical horseshoe vortex system caused by the adverse pressure gradient of the stagnating flow is developed, Figs. 2(a) and 2(b). At flow section Z/H=0 (Fig. 2(a)), and according to the flow considerations of Martinuzzi and Tropea (1993), this three-dimensional swirl is delimited by the upstream separation line ln_A, and line ln_C near the upstream side of the prism. The horseshoe vortex centre is underlined with the line ln_B. In the symmetric flow section, Fig. 2(b), up to a stagnation point A_1, the fluid skirts the obstacle. Down this point, the fluid feeds the horseshoe vortex system. According to Backer (1991) for this flow patterns (moderate Reynolds number and thin boundary layer), the observed upstream close flow structure is stationary and composed of four vortices.

On the obstacle sides (section Z/D=0) Fig. 2(a), a low pressure region generates a close three-dimensional and unsteady recirculation vortex structure. Beyond Z/D=0.15, this vortex system is opened toward the wake and is unsteady.

Downstream the block sharp upper face edge, a recirculation region, due to the main streamline take off, lies flat on the top block. This recirculation region not attached to the obstacle involves the fluid, located in the wake, to go back by aspiration. Because of strong shearing interactions between the main positive flow and this opposed recirculation, vortices are regulary generated in this top block zone and shed towards the wake (Fig. 3). A Z/D=0.3 topology study and the 3D visualization of this flow area (Figs. 4(a) and 4(b)) allow to better discern the three

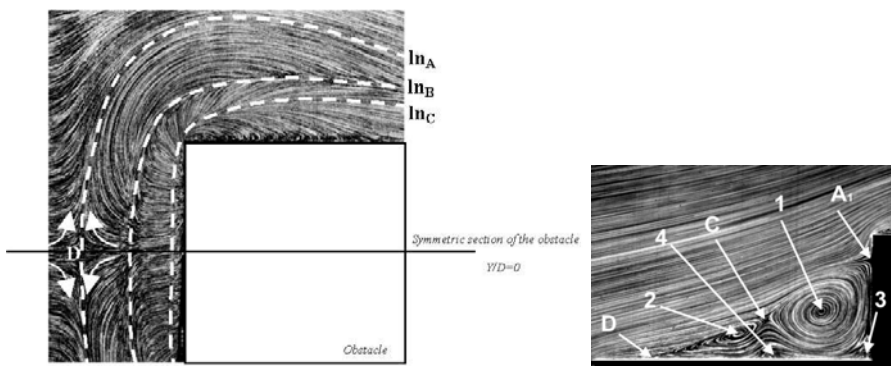

(a) Horseshoe vortex visualization in the section Z/D=0.

(b) Horseshoe vortex visualization in the symmetry plane of the obstacle (Y/D=0).

Fig. 2. Particle visualizations and topology.

dimensional shape of the structure, originated in the upstream sharp corner and delimited by the main flow and the top box face. It is composed by two rotational structures at top block face which defined the bases of the symetrically 3D vortex system, in an arch form. This complex, three dimensional and unsteady structure stretches towards the wake until it is disunited from its bases (Fig. 4(b)). Consequently, a cyclic vortex shedding phenomena is generated at a frequency of 0.24 Hz.

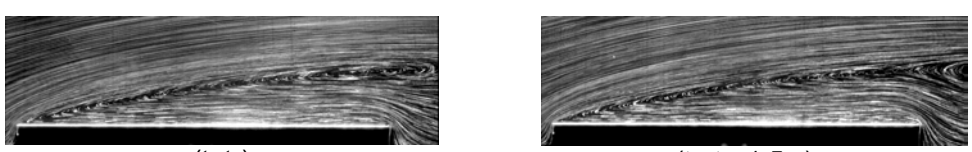

($t=t_0$) ($t= t_0+1.5$ s)

Fig. 3. Particle visualizations at the top of the obstacle in the section Y/D=0.

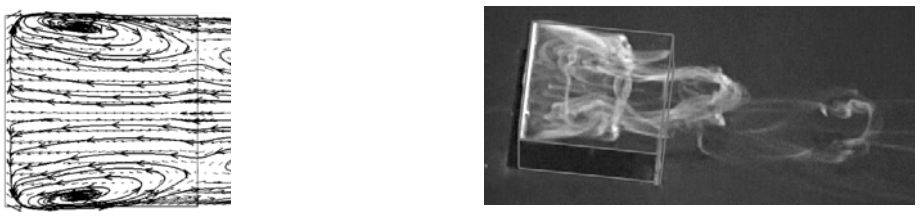

(a) PIV streamlines in the plane Z/D=0.3.

(b) 3D visualization by continuous dye-emission.

Fig. 4. Arch vortex system at the top of the obstacle.

Downstream the obstacle, the horseshoe vortex separation line ln_A continues. Inside the line, a low pressure region exists and an over complex and three-dimensional swirling system is observed. In the section Z/H=0.15 the particle visualization techniques, Fig. 5, emphasis two different flow topologies: a symmetric and an unstable dissymmetric ones.

The (O/XZ) section flow allows to better understand the downstream flow dynamic. In the section Y/D=0, 2C-PIV measurements display two different vortex evolutions, Fig. 6. In a process 1, a vortex originating from the top of the block is detected in the near wake. In a first step, this vortex separates the top block region, grows and its center altitude decreases. Afterwards, its position becomes stable at X/D=1.68, Z/D=0.39. Next, at time $t=t_0$, a second vortex also coming from the top of the obstacle is visualized downstream and merges with the first vortex at time $t=t_0+1.482$ s. This new rotational structure generated escapes towards the wake. Its center comes closer to the obstacle ground support. Moreover, in this process 1, the vortex structure is defined by an acceleration of the flow according to the Z direction. This acceleration is characterized by an evolution of the instantaneous components w up to the center of the vortex. In a process 2 of the vortex shedding, no similar merging process is visualized. The vortex originates from the top block, escapes towards the wake and keeps the same Z/D altitude during its near wake space evolution, Fig. 6(b). Contrary to the process 1, the process 2 mechanism is not cyclic.

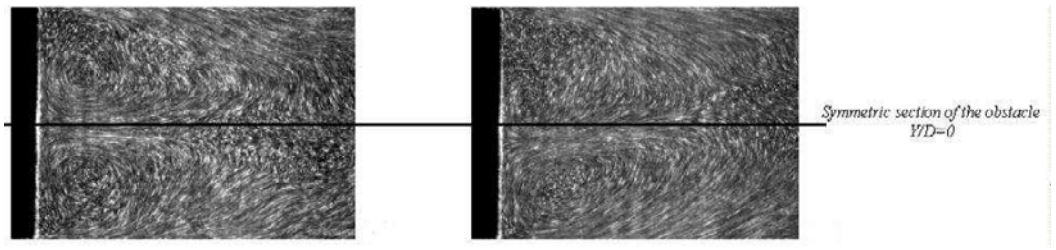

(a) Symmetric topology (b) Dissymmetric topology

Fig. 5. Particle visualizations in the section Z/D=0.15 downstream the obstacle.

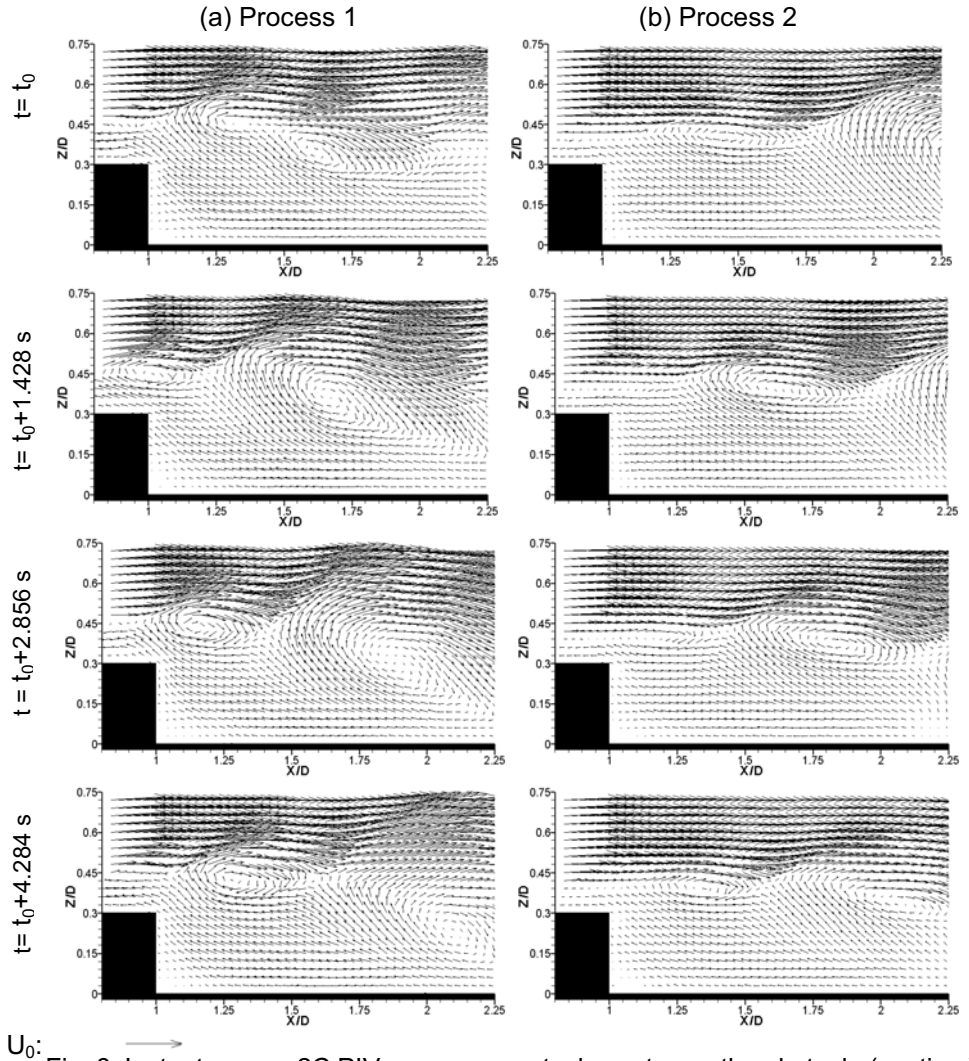

Fig. 6. Instantaneous 2C PIV measurements downstream the obstacle (section Y/D=0).

In order to better relate the three-dimensional near wake topology, 3C PIV measurements have been carried out in the plan (O/XZ) with Y/D=1/6, Fig. 7. This experimental investigation allows to highlight the previous three-dimensional spatial evolution of the two vortex shedding processes. In the first case, the vortex originates from the top of the model, merges with a second vortex to create a quasi-plane rotational structure with low out-of-plane component gradients. On the contrary, for the process 2 (dissymmetric one), the rotational structure escapes towards the wake with significant out-of-plane component values. Those distributions of the v component underline the two different three-dimensional spatial evolution of the two vortex shedding processes and allow to understand, in particular, the process 2.

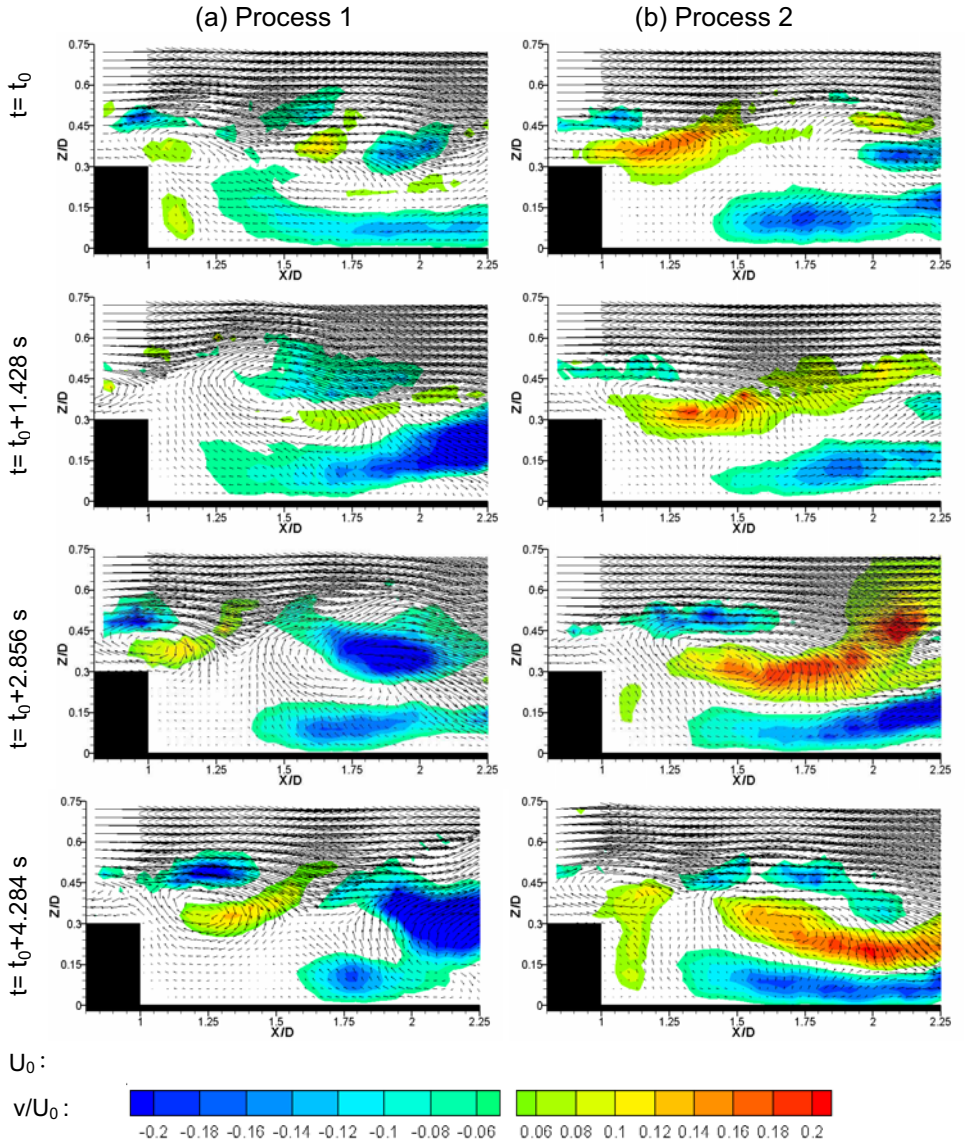

Fig. 7. Instantaneous 3C PIV measurements downstream the obstacle (section Y/D=1/6).

4. Temporal, Spatial and Spatio-Temporal Correlation Functions

In order to link the previous section quantitative results with the stability of the vortex shedding process, the temporal, spatial, spatio-temporal correlation functions are considered. Besides different authors - Kähler et al. (2000), Santa Cruz et al. (2000) - already have employed the correlation functions in order to obtain some quantitative flow structure evolutions based on experimental PIV data measurements. So to lead to the flow dynamic and the shedding process understanding with coherent time and space resolutions the different double fluctuation velocity correlations have been calculated by means of a continuous acquisition of the velocity. In the section Y/D=0, according to the flow dynamic, 2,500 measurements of the instantaneous 2C velocity flow fields with an acquisition frequency of 25 Hz have been used. Consequently, this large data set makes it possible to understand the flow dynamic and the evolutions of the vortices which escape towards the wake with coherent time and space resolutions. Although the SPIV makes it possible to acquire the 3 velocity components, downstream the obstacle, the fluctuations w' (x, y, z, t) give the best flow dynamic information in this results. Consequently, only the temporal correlation functions $R_{w'w'}(t)$ is explained

in details in order to identify and to understand vortex shedding evolutions.

Investigations are made on four selected points in the near wake domain, Fig. 8. One is set at (P_1) X/D=1.065; Z/D=0.356, close downstream the obstacle to exclusively characterize the vortex evolution originating from the top of the parallelepiped. The second point (P_2) is positioned at X/D = 1.438; Z/D=0.386 and defines the place of the vortex merging phenomena, where the standard deviation w_{RMS} is maximum. The third (P_3) and fourth (P_4) points (X/D=2.115; Z/D=0.281 and X/D=2.115;Z/D=0.431) are selected to allow to discern the trajectory evolutions of the two specific vortex shedding processes.

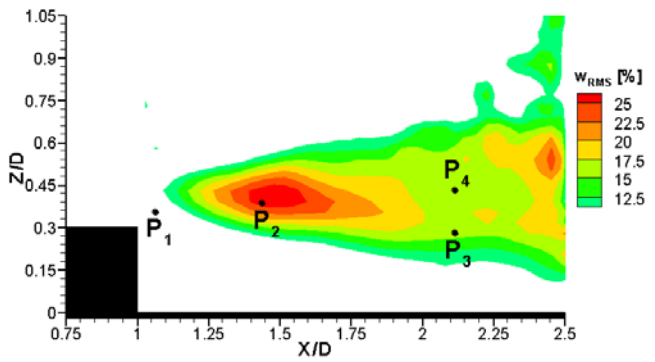

Fig. 8. W root mean square distribution and the position of the 4 points.

For those four points, the temporal correlation coefficient $R_{w'w'}(t)$ evolutions are plotted Fig. 9. On P_1, Fig. 9(a), a periodic evolution exists which highlights the vortex progress originating from the top of the block. The vortices coming from the higher face of the obstacle escape towards the wake in a regular shedding phenomena with a frequency equal to 0.24 Hz (period time τ_P=4.2 seconds). Because of the two distinct vortex shedding processes, previously displayed, the different $R_{w'w'}(t)$ plotting peak magnitudes are not identical. This constatation founds expression in a relatively weak dependence between the fluctuations w'(t) and w'(t+τ_P).

On P_2, Fig. 9(b), a main peak is evident at the time τ_{t1}=7.8 seconds, a second one appears at the time τ_{t2}=4.2 seconds. This statement on point P_2 is closely set in the near wake zone where vortices can merge confirms the fact that the vortex process 1 is dominating. Indeed, during this process, a vortex originating from the top of the model sheds towards the wake at a time t. Then, it becomes stable near the place P_2. At time t+τ_P, a second vortex comes downstream. At time t+2.τ_P, those two vortices merge. Differently, and for the process 2, at this step the second vortex escapes and goes straight towards the wake without merging phenomena. So, the main peak at time τ_{t1}=7.8 seconds underlines the merging phenomena which exists during the vortex process 1. The secondary peak at time τ_{t2} highlights the vortex shedding process 2. Moreover, and as for the flow visualizations, the maximum peak magnitude obviously expresses the fact that the process 1 is more frequently observed.

According to the process modes, the $R_{w'w'}(t)$ evolutions determined at the points P_3 and P_4, Figs. 9(c) and 9(d), bring the direction of the rotational structures shedding. Indeed at P_3, only one peak is observed at time τ_{t1}=7.8 seconds. On P_4, a two peaks $R_{w'w'}(t)$ evolution is computed. It was previously exhibited that during the vortex process 2 evolution, the vortex sheds towards the wake, keeps its core at the same altitude during its space evolution. In the process 1, the center of the rotational structure makes its way downwards the plane block support. Consequently, at P_3, only the process 1 shedding dynamic can be observed.

The distribution of the spatio-temporal correlation function $R_{w'w'}(t+\tau)$, Fig.10, for τ=4 seconds, is determined close to the point P_2, where the vortex coalescence phenomena takes place. This correlation map highlights the vortex space and time evolutions. Three distinct areas, Fig. 10, can be distinguished. According to the process 1, a downward vortex trajectory evolution generates a significiant spatio-temporal correlation coefficients area 1. Moreover, for this mechanism, the dynamic of the vortex shedding generates a coherent fluid structure enlargement which imposes a positive w velocity gradient in the noted area 3. In the process 2, the vortex translation (constant altitude) generates the spatio-temporal correlation coefficients area 2. So, in the model near wake

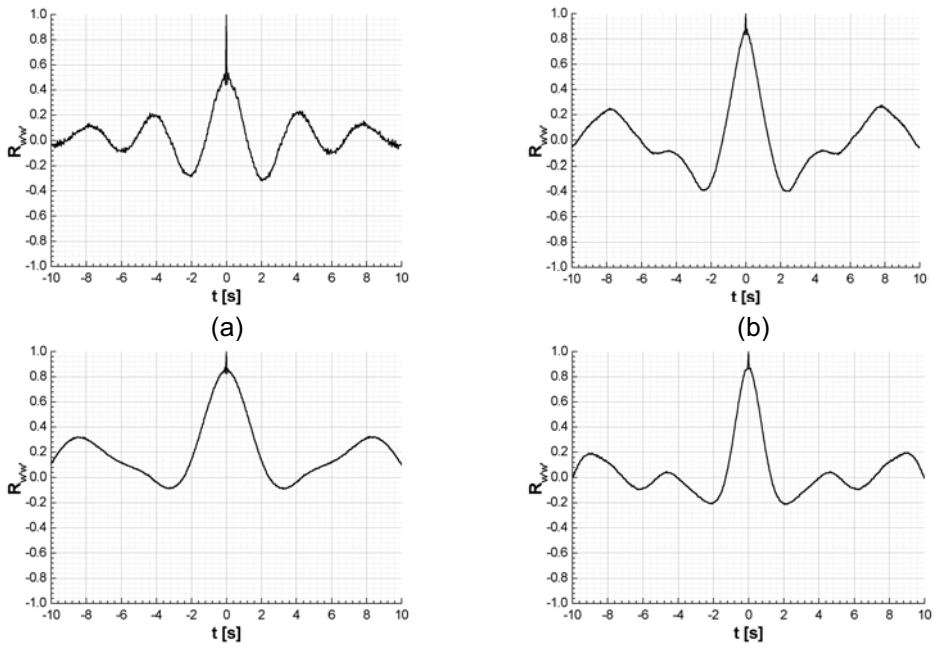

Fig. 9. Temporal correlation evolution of Rw'w'(t) at the 4 points: (a) P1, (b) P2, (c) P3, (d) P4.

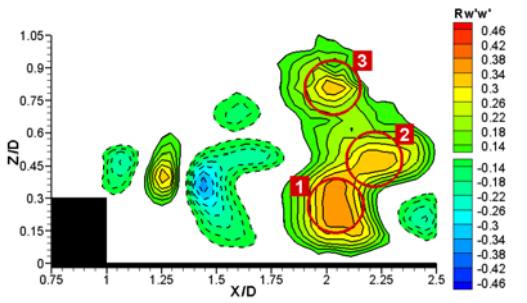

Fig. 10. Rw'w'(t+τ) spatio-temporal correlation map with τ=4 s, calculating from the point P2.

zone, the spatio-temporal correlation function calculation makes it possible to highlight the two trajectory types of the random top block vortex shedding mechanisms.

To make a three-dimensional analysis of the influence of v/U_0, the perpendicular component to the experimental lighting plan Y/D=1/6, the temporal correlation functions $R_{u'u'}(t)$, $R_{v'v'}(t)$ and $R_{w'w'}(t)$, Fig. 11, are plotted. At the difference of the preceding results which are done with a only one and continuous PIV acquisition, these graphs were carried out starting from two series of 200 instantaneous sequential 3C velocity fields which cover an experimental time of 20 seconds. The correlation coefficients are computed at X/D=1.763, Z/D=0.450 spot of the plan where the standard deviation w_{RMS} is maximum. During the first series of the 3C PIV measurements, Fig. 11(a), only few vortex shedding process 2 dynamic is detected. Contrariwise, during the second series, Fig. 11(b), the flow is characterized essentially by a dissymmetrical vortex shedding process, the process 2. Note the shape similarities of the three temporal correlation functions $R_{v'v'}(t)$, $R_{u'u'}(t)$ and $R_{w'w'}(t)$ which display that, in the thin volume measurement domain, the vortex evolutions are defined by significiant v components. So, it appears that the out-of-plane component contribution is essential to understand the flow dynamics and its swirling evolutions. Moreover, for both 3C PIV measurement series hold, the 200 instantaneous sequential velocity fields are fully different and each series more particularly characterizes each flow dynamic modes previously described. So, according to the PIV set up, in order to accurately study this flow dynamic by means of correlation functions, it is essential to acquire and store a maximum of continuous velocity field series covering the largest possible time of the flow evolution.

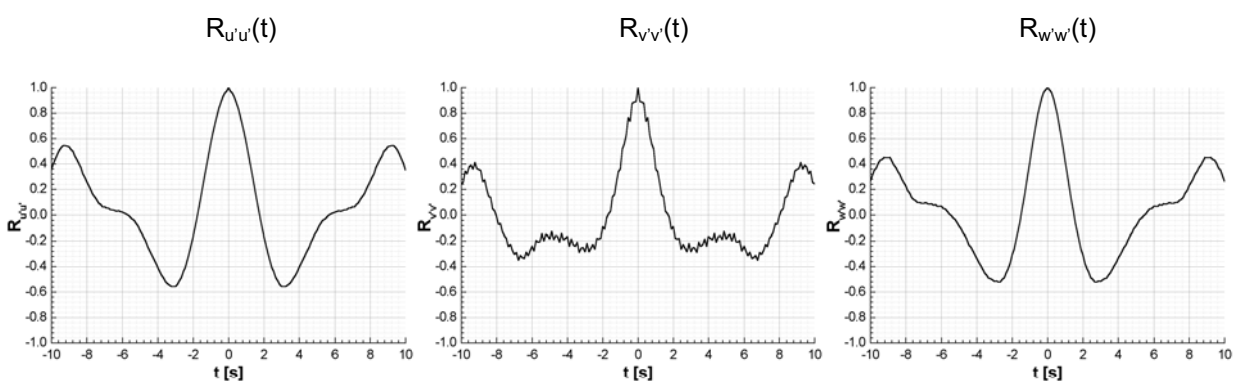

(a) First series of 200 velocity fields

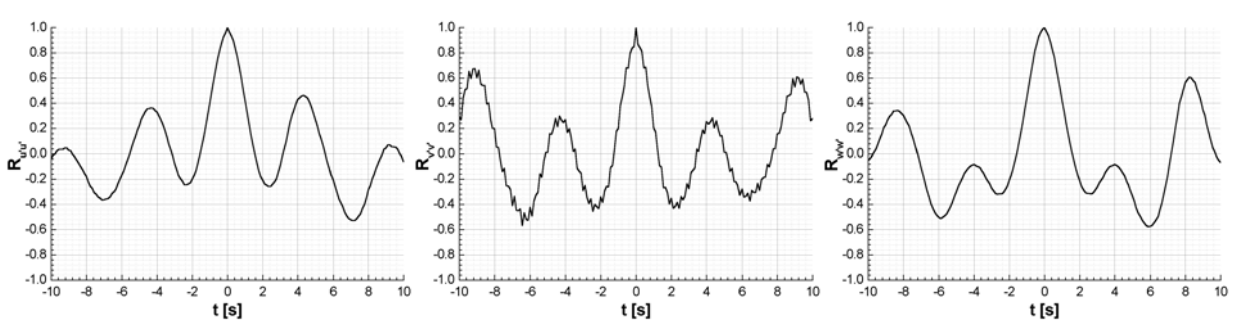

(b) Second series of 200 velocity fields

Fig. 11. Temporal correlation Ru'u'(t) Rv'v'(t) Rw'w'(t) evolutions in the plan Y/D=1/6.

5. Conclusion

The analyses of qualitative and quantitative experimental data of the unsteady three-dimensional established flow around a block are exposed. Particulary, two vortex shedding processes have been noted by particles visualizations and 2C or 3C PIV instantaneous measurements. Moreover, and in order to understand those wake dynamics, a study of correlation coefficients has been performed. This statistical analyse and instantaneous flow visualizations study have been allowed to detail the space and time evolutions of the vortex shedding according to the process.

Upstream the obstacle, the flow is characterized by a stationary horseshoe vortex system composed of four vortices. On the close obstacle sides, ovalized rotational structures are generated. On the top of the parallelepiped, a detachment zone exists with no flow reattachment on the higher face. Consequently, downstream the obstacle, a complex flow topology is visualized. In this flow domain, a return of fluid per aspiration on the higher part of the obstacle is generated. As a result of the strong shearing regions which are created by interaction between an accelerated flow according to a positive direction and the return of fluid according to the opposed direction, some vortices are created and escape towards the wake. The analysis of instantaneous 2C and 3C PIV velocity fields and particles visualizations have emphased two vortex shedding processes. According to the process 1, the flow topology stays symmetric. An arch form swirl originates from the top of the obstacle, moves downstream, and stabilizes in the near wake. Then, a second vortex appears downstream the obstacle. The two vortices merge, and, a new rotational structure is generated and escapes towards the wake. According to the process 2 mechanism, the flow topology is dissymmetrical and no mixing phenomenon is visualized. Moreover, the vortex process 1 evolution and the associate flow dynamic seems to be dominant.

The temporal, space, spatio-temporal correlation coefficients of double fluctuation velocity computing on a continuous acquisition covering 100 seconds of experiments have been calculated. With thoses statistical investigation tools, the trajectories of the vortices and the frequencies, according to the shedding mechanisms, have been obtained. The vortices originated from the higher region of the obstacle shed in the wake with a frequency of 0.24 Hz. Downstream the obstacle, in the process 1 evolution, after the coalescence phenomenon, the altitude of the center of the rotional

structure decreases during the vortex evolution downwards the wake. During the process 2, the vortex sheds in the wake escapes towards the wake at a constant altitude Z/D.

References

Baker, C. J., The oscillation of horseshoe vortex systems, Journal of Fluid Engineering, 113 (1991), 489-495.
Becker, S., Lienhart, H. and Durst F., Flow around three-dimensional obstacles in boundary layers, Journal of Wind Engineering and Industrial Aerodynamics, 90 (2002), 265-279.
Calluaud, D. and David, L., Stereoscopic particle image velocimetry measurements of the flow around a surface-mounted block. Experiments in Fluids, 36-1 (2004), 53-61.
Castro I. P. and Robins A. G., The flow around a surface-mounted cube in uniform and turbulent streams, Journal of Fluid Mechanics, 79-2 (1977), 307-335.
Castro, I. P. and Dianat, M., Surface flow patterns on rectangular bodies in thick boundary layers, Journal of Wind Engineering and Industrial Aerodynamics, 11 (1983), 107-119.
Hunt, J. C. R., Abell, C. J., Peterka, J. A. and Woo, H., Kinetical studies of the flows around free or surface-mounted obstacles, applying topology to flow visualization, Journal of Fluid Mechanics, 86-1 (1978), 179-200.
Kähler, C. J., Stanislas, M., Dewhirst, T. and Carlier, J., Investigation of the spatio-temporal flow structure in a log-law region of a turbulent boundary layer by means of multi-plane stereo PIV, In: Adrian R. J., Durao D. F. G., Durst F., Heitor M. V., Maeda M., Whitelaw J. H. (eds) Laser technique for fluid mechanics (2002).
Larousse, A., Martunizzi, R. J. and Tropea, C., Flow around surface-mounted, three-dimensional obstacles, Proceedings of the 8th Symposium on turbulent Shear flows (Technical University of Munich, Germany), (1991).
Martunizzi, R. J. and Tropea, C., The flow around surface-mounted obstacles placed in a fully developed channel flow, Journal of Fluid Engineering, 115 (1993), 85-92.
Martunizzi, R. J., Tropea, C. and Volkert, J., Observation of the flow over prismatic obstacles in a fully developed channel flow, IUTAM Symposium of Bluff Body Wakes, Dynamics and Instabilities (Göttingen, Germany), (1992).
Prasad, A. K., Stereoscopic particle image velocimetry, Experiments in Fluids, 29 (2000), 103-116.
Prasad, A. K. and Jensen K., Scheimpflug stereocamera for particle image velocimetry in liquid flows, Applied Optics, 34-30 (1995), 7092-7099.
Santa Cruz, A., Pécheux, J. and David, L., Half cylinder wake representation by POD to evaluate the influence of a splitter plate, Proceedings of EUROMECH (Rouen), 411 (2000).
Scarano, F., Theory of non-isotropic spatial resolution in PIV, Experiment in Fluids, 35-3 (2003), 268-279.
Schofield, W. H. and Logan, E., Turbulent shear flow over surface mounted obstacles, Journal of Fluid Engineering, 112 (1990), 376-385.
Sousa, J. M. M., Turbulent flow around a surface-mounted obstacle using 2D-3C DPIV, Experiments in Fluids, 33 (2002), 838-853.
Vlachos, P. P. and Hajj M. R., A time-resolved DPIV study of the unsteady character of the flow over a surface-mounted prism, Journal of Wind Engineering and Industrial Aerodynamics, 90 (2002), 543-553.

Author Profile

Damien Calluaud: He received his Fluid Mechanic Ph.D. in 2003 at the Poitiers University (France). He works in the Aerodynamic Laboratory of Poitiers. His research interests are three component velocity technique and algorithm developments by PIV , quantitative visualization, topology analyses, unsteady

Laurent David: He is an Assistant Professor in Fluid Mechanics, and he develops for the L.E.A. optical measurements. His research topics are some experimental investigations of near wake flows and cross flows for aerodynamic and combustion applications. He teaches at the Institute of Technology of Poitiers.

Alain Texier: He is a Full Professor in Fluid Mechanic and a Director of the Technological Institute of Poitiers (France). His main team research topics in the Aerodynamic Laboratory of Poitiers are experimental fluid simulations, topology and dynamic wake understanding and control.